Time-dependent density-functional-theory calculation of high-order-harmonic generation of H_2

Xi Chu
Center for Biomolecular Structure and Dynamics, Department of Chemistry and Biochemistry, The University of Montana, Missoula, Montana 59812, USA

Gerrit C. Groenenboom
Radboud University Nijmegen, Institute for Molecules and Materials, Heyendaalseweg 135, 6525 AJ Nijmegen, The Netherlands
(Received 28 February 2012; published 1 May 2012)

The observation of the isotope effect in the high-order-harmonic generation (HHG) of H_2 presents a challenge for time-dependent density-functional-theory (TDDFT) methods, since this effect is related to the dynamics of the ion created in the tunneling ionization step of HHG and it depends on the harmonic order. As an initial step toward describing this effect within current computational capacity, we benchmark a method in which the nuclear and electronic degrees of freedom are separated and both treated quantum mechanically. For the electrons two TDDFT formalisms are adopted. Although the ion-dynamics effect is not described in our method, it reproduces the measured D_2-to-H_2 HHG ratios up to the 25th harmonic when the 35th is the classical cutoff. Beyond the 25th harmonic, however, our results show substantial deviation and are sensitive to the laser intensity. A higher intensity reproduces the experimental results. Analysis reveals an R-dependent phase factor as the cause of the isotope effect in our calculation. We isolate this phase factor and propose a strong-field-approximation-phase model, which reproduces experimental data, including those for which the ion-dynamics model has to be further modified. We show that the model that we propose is intrinsically related to the ion-dynamics model. Our model provides a correction to the TDDFT approach when the ion-dynamics effect becomes significant. It also indicates that the isotope effect is not only a probe for the ion created by the external field but is ultimately a more useful probe for the ground-state nuclear wave function. For all molecules whose vertical ionization potential strongly depends on the nuclear geometry, HHG may serve as a sensitive ultrafast probe of nuclear dynamics.

DOI: 10.1103/PhysRevA.85.053402 PACS number(s): 33.80.Rv, 31.15.ee, 33.80.Eh, 33.90.+h

I. INTRODUCTION

High-order-harmonic generation (HHG) [1,2] is a highly nonlinear strong-field phenomenon that has been intensively studied for its optical applications in creating XUV lasers and attosecond pulses since its discovery. In recent years HHG of molecules has been studied for its potential to probe, with subfemtosecond temporal resolution, nuclear dynamics including vibration [3–7] and dissociation [7]. The foundation of these applications is the sensitivity of HHG emission to the nuclear geometry and motion. So far, the involvement of multiple molecular orbitals [6,7] and two-center interference [5,7] have been proposed as causes for the large oscillation of the HHG intensity in response to geometry changes in molecules. Further theoretical studies that detail the relation of molecular structure and dynamics with their HHG can contribute to the maturity of the application of HHG as a subfemtosecond molecular dynamics probe.

Currently, quantitative prediction of HHG largely relies on the semiclassical Lewenstein model [8]. This model is consistent with the well-accepted three-step model [9,10], which consists of the generation of a free electron through tunneling ionization, the acceleration of this electron, and its recombination with the parent ion while emitting harmonics. Present semiclassical methods usually ignore all excited states, the depletion of the ground state, and the interaction between the active electron and the parent ion in the continuum. The single-active-electron (SAE) approximation is usually further applied. As such, all the electronic structure information is embedded in the highest occupied molecular orbital (HOMO) function and the ionization potential (I_p). Such calculations can resolve the alignment-angle-dependent HHG signals [11] and thus reveal the relation between the tomography of the HOMO and the HHG signal. The limitation of these methods is that the multielectron dynamics, the effect of multiple orbitals, and the role of excited states cannot be studied. In particular, the roles of multiple orbitals and multielectrons have been observed experimentally [12,13].

A quantum-mechanical approach with all electrons included provides a more complete description of the process, although such a method requires extremely large-scale computation. This method has to be able to treat the ground and excited states together with the continuum with sufficient accuracy. It also should be able to describe other strong-field processes that accompany HHG, including ionization and excitation. In this work we employ time-dependent density-functional theory (TDDFT) [14]. The advantage of TDDFT is that it is in general less costly in terms of computation, while electron correlation is accounted for to some extent.

An important issue that is yet to be resolved is the coupling between the electronic and nuclear degrees of freedom. As the lightest molecule, hydrogen is particularly subject to this problem. In 2006 Baker *et al.* [4] observed that D_2 gives a stronger HHG signal than H_2 and that the ratio increases with the harmonic order. Lein had predicted this effect earlier by assuming that the nuclear wave function propagates on the ion potential after ionization in each half optical cycle [15]. The propagation time depends on the harmonic order n. It is assumed that HHG only weakly depends on the interatomic distance R, so that the R dependence is ignored and an isotope-dependent nuclear correlation function is factored out. The HHG signal

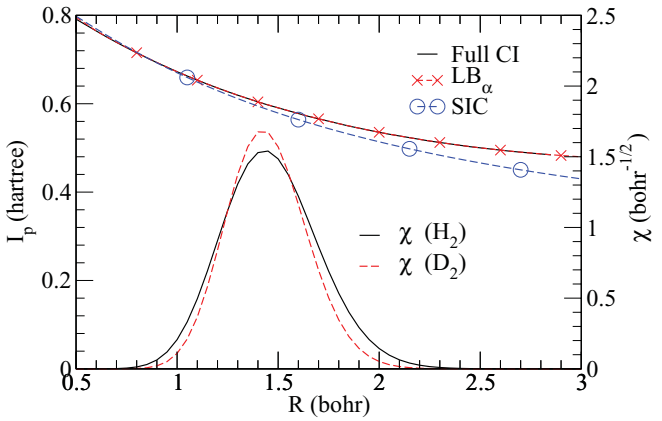

FIG. 1. (Color online) The vertical I_p calculated by full CI, LB$_\alpha$, and SIC methods together with the ground vibrational wave functions of H_2 and D_2.

is then reduced by the square of the nuclear autocorrelation function at the time of recombination. Since D_2^+ vibrates more slowly than H_2^+, its HHG intensity is larger. This model was applied to the experimentally selected short trajectories for which the recollision time increases with the harmonic order [16], explaining why the signal ratio increases with n.

Ignoring the R dependence of the electron dynamics in Lein's ion-dynamic model is the crucial assumption that makes it possible to separate the electron and nuclear degrees of freedom. In a 2008 follow-up experiment, Baker *et al.* [5] remeasured the isotope effect with different laser intensities and a longer pulse duration. They demonstrated that this model had to be extended by postulating a dynamic two-center interference effect, which is R dependent. Only calculations that treat nuclei as well as electrons fully quantum mechanically can describe the coupled electron and nuclear dynamics. Lein performed such calculations on H_2, where an effective potential is employed to reduce the electron dynamics to two dimensions, but coupling to the nuclear degrees of freedom is treated exactly [15]. For larger molecules, however, full quantum calculations are prohibitively large.

In this study, instead of ignoring the R dependence of HHG while approximating the nuclear dynamics by having it adiabatically evolve on a Born-Oppenheimer ion potential, we treat the R dependence with our TDDFT method but assume a stationary nuclear wave function. According to the ion-dynamics model, we should expect no isotope effect in this treatment. However, as shown in Fig. 1, the nuclear wave functions of the ground states of H_2 and D_2 are different, and if HHG strongly depends on R, then an isotope effect may arise. This work is motivated by the following considerations: (1) For lower harmonics, i.e., when the energy of the emitted photon is lower than I_p, a stationary nuclear wave function should be valid, since the three-step model does not apply here and the molecule does not go through tunneling ionization. (2) According to the ion-dynamics model, the nuclear autocorrelation function is close to 1, when the recombination time $\tau(n)$ is small, and it decreases with increasing n. So we expect the error caused by ignoring the nuclear dynamics to increase with n. By benchmarking the isotope effect calculated with our methods against the experimental values, we can estimate the highest harmonic order for which the stationary nuclear approximation is valid. Such a study will shine light on the accuracy of TDDFT calculations of HHG of other hydrogen-containing molecules. (3) By understanding the nature of the R dependence, we may propose a model that empirically incorporates effects of both the R dependence and the ion dynamics.

II. TIME-DEPENDENT DENSITY-FUNCTIONAL THEORY FOR MOLECULE–STRONG-FIELD INTERACTIONS

A TDDFT method has been developed for treating diatomic molecules interacting with a linearly polarized laser, whose polarization direction is parallel to the molecular axis [17–19]. Later this work was extended to treat arbitrary polarization directions for the study of the anisotropy of ionization and HHG [20–22]. We use the approach of Ref. [23], which includes multiple electronically excited states, the depletion of the ground state, and the interaction between the active electron and the parent ion in the continuum. The exchange and correlation functionals we use here are Leeuwen-Baerends (LB)$_\alpha$ [24] and self-interaction correction (SIC) [17], whose accuracy has been extensively benchmarked [17,18,21,23]. We refer to the TDDFT methods using these two functionals as the TDLB$_\alpha$ method and the TDSIC method, respectively.

Details of the TDSIC and TDLB$_\alpha$ descriptions of a homonuclear diatomic molecule in an intense laser field are given in previous articles [17,18,23]. Here we give a brief account of their formalisms.

The electron density at electron coordinate $\mathbf{r}$ and time t is

$$\rho(\mathbf{r},t;R) = \sum_\sigma \sum_{i=1}^{N_\sigma} \rho_{i\sigma}(\mathbf{r},t;R) = \sum_\sigma \sum_{i=1}^{N_\sigma} \psi^*_{i\sigma}(\mathbf{r},t;R)\psi_{i\sigma}(\mathbf{r},t;R), \quad (1)$$

where i is the orbital index and σ is the spin index. The spin orbital $\psi_{i\sigma}$ satisfies the one-electron Schrödinger-like equation, in atomic units,

$$i\frac{\partial}{\partial t}\psi_{i\sigma} = \hat{H}(\mathbf{r},t;R)\psi_{i\sigma} = \left[-\frac{1}{2}\nabla^2 + v_{\mathrm{eff},\sigma}(\mathbf{r},t;R)\right]\psi_{i\sigma} \quad \text{for} \quad i = 1,2,\ldots,N_\sigma, \quad (2)$$

where N_σ is the number of electrons that have σ spin. The effective potential $v_{\mathrm{eff},\sigma}$ of the TDSIC functional for a homonuclear diatomic molecule [17] is

$$v^{\mathrm{SIC}}_{\mathrm{eff},\sigma} = -\frac{Z}{|\mathbf{R}_1-\mathbf{r}|} - \frac{Z}{|\mathbf{R}_2-\mathbf{r}|} + \int d^3\mathbf{r}'\frac{\rho(\mathbf{r}',t;R)}{|\mathbf{r}-\mathbf{r}'|} + \mathbf{E}(t)\cdot\mathbf{r} + V_{\mathrm{SIC},\sigma}(\mathbf{r},t;R), \quad (3)$$

where $\mathbf{E}(t)$ is the electric field of the laser, and for a dc field it is constant. $\mathbf{R}_1$ and $\mathbf{R}_2$ are the coordinates of the two nuclei, with nuclear charges Z,

$$V_{\mathrm{SIC},\sigma} = \sum_i \frac{\rho_{i\sigma}(\mathbf{r},t;R)}{\rho_\sigma(\mathbf{r},t;R)}\left\{v_{i\sigma}(\mathbf{r},t;R) + \left[\overline{V}^i_{\mathrm{SIC},\sigma}(R,t) - \overline{v}_{i\sigma}(R,t)\right]\right\}, \quad (4)$$

$$v_{i\sigma} = V_{\rm xc}[\rho_\uparrow(\mathbf{r},t;R),\rho_\downarrow(\mathbf{r},t;R)] - \iiint d\mathbf{r}'\frac{\rho_{i\sigma}(\mathbf{r}',t;R)}{|\mathbf{r}-\mathbf{r}'|} - V_{\rm xc}[\rho_{i\sigma}(\mathbf{r},t;R),0], \quad (5)$$

and

$$\overline{V}^{i}_{{\rm SIC},\sigma} = \langle\psi_{i\sigma}|V_{{\rm SIC},\sigma}(\mathbf{r},t;R)|\psi_{i\sigma}\rangle, \quad (6)$$

$$\overline{v}_{i\sigma} = \langle\psi_{i\sigma}|v_{i\sigma}(\mathbf{r},t;R)|\psi_{i\sigma}\rangle. \quad (7)$$

For the TDLB$_\alpha$ functional, we have

$$v^{{\rm LB}_\alpha}_{{\rm eff},\sigma} = -\frac{Z}{|\mathbf{R}_1-\mathbf{r}|} - \frac{Z}{|\mathbf{R}_2-\mathbf{r}|} + \iiint d\mathbf{r}'\frac{\rho(\mathbf{r}',t;R)}{|\mathbf{r}-\mathbf{r}'|} + \mathbf{E}(t)\cdot\mathbf{r} + V_{{\rm LB}_\alpha,\sigma}(\mathbf{r},t;R) \quad (8)$$

and

$$V_{{\rm LB}_\alpha,\sigma} = \alpha v^{\rm LSDA}_{x\sigma}(\mathbf{r},t;R) + v^{\rm LSDA}_{c\sigma}(\mathbf{r},t;R) - \frac{\beta x^2_\sigma(\mathbf{r},t)\rho^{1/3}_\sigma(\mathbf{r},t;R)}{1+3\beta x_\sigma(\mathbf{r},t)\ln\left\{x_\sigma(\mathbf{r},t;R)+\left[x^2_\sigma(\mathbf{r},t;R)+1\right]^{1/2}\right\}}, \quad (9)$$

which contains two empirical parameters α and β.

In Eq. (9), $v^{\rm LSDA}_{x\sigma}$ and $v^{\rm LSDA}_{c\sigma}$ are the local-spin-density approximation (LSDA) exchange and correlation potentials, which do *not* have the correct asymptotic behavior. The last term is the gradient correction with $x_\sigma(\mathbf{r}) = |\nabla\rho_\sigma(\mathbf{r})|/\rho_\sigma(\mathbf{r})^{4/3}$, which ensures the proper long-range asymptotic behavior $v^{{\rm LB}\alpha}_{{\rm xc}\sigma} \to -1/r$ as $r \to \infty$.

III. HHG POWER-SPECTRUM CALCULATIONS

The numerical solution of the time-dependent equations is detailed in a recent publication [23]. Once the electron density $\rho(\mathbf{r},t;R)$ is obtained, the induced dipole moment and dipole acceleration can be determined, respectively, as

$$d(R,t) = \int \rho(\mathbf{r},t;R)z\,d^3\mathbf{r} \quad (10)$$

and

$$a(R,t) = \sum_\sigma \int \rho_\sigma(\mathbf{r},t;R) \times \left[-\frac{\partial V_{{\rm eff},\sigma}(\mathbf{r},t)}{\partial z} + \frac{\mathbf{E}(t)\cdot\mathbf{r}\sin(\omega t)}{z}\right] d^3\mathbf{r}. \quad (11)$$

The HHG power spectrum is related to the Fourier transform of the corresponding time-dependent dipole moment or dipole acceleration:

$$d(R,\omega) = \frac{1}{t_f-t_i}\int_{t_i}^{t_f} d(R,t)e^{-i\omega t}dt \quad (12)$$

and

$$a(R,\omega) = \frac{1}{t_f-t_i}\int_{t_i}^{t_f} a(R,t)e^{-i\omega t}dt = -\omega^2 d(R,\omega), \quad (13)$$

where ω is the angular frequency of the emitting photon. For homonuclear diatomic molecules, when $\omega = n\omega_0$, where ω_0 is the angular frequency of the driving field and $n = 1,3,5,\ldots$, there is a spur of HHG emission. Numerically the density at the long range is more important for the dipole while the density at the short range is more important for the acceleration. Their agreement is proof of the quality of $\rho(\mathbf{r},t;R)$ on the spatial grid.

We separate electronic and nuclear motion and treat both quantum mechanically. The spectral density, in atomic units, is computed as

$$S(\omega) = \frac{3}{2\pi c^3}|\langle\chi(R)|a(R,\omega)|\chi(R)\rangle|^2 = \frac{3}{2\pi c^3}|\langle a(\omega)\rangle|^2, \quad (14)$$

where c is the speed of light. The nuclear wave function $\chi(R)$ is computed with the sinc-function discrete-variable-representation (DVR) method [25,26] for the ground-state potential of H_2 [27]. We calculate the dipole acceleration on an equally spaced grid with 50 points for $0.6a_0 \leqslant R \leqslant 3.0a_0$, by running TDDFT calculations on each point. We then evaluate the integral numerically, with equal weights for each grid point. A TDDFT calculation for a single value of R takes about two hours on a workstation.

IV. HHG OF H_2 AT FIXED INTERNUCLEAR DISTANCES

We consider a linearly polarized laser field with a $\sin^2$ pulse shape, 20 optical cycles in pulse length, and a laser intensity of 2×10^{14} W/cm^2 at a wavelength of 800 nm. The electric field polarization is parallel to the molecular axis. This parallel orientation significantly reduces the size of the computation because the axial symmetry is conserved.

In Fig. 2 we show $|a(R_{\rm eq},\omega)|^2$ calculated with the TDSIC and TDLB$_\alpha$ methods together with $|\langle a(\omega)\rangle|^2$ for the odd

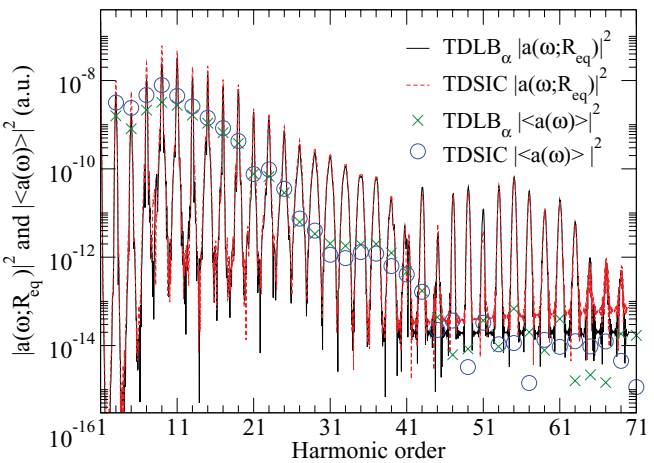

FIG. 2. (Color online) Squared dipole acceleration $|a(R_{\rm eq},\omega)|^2$ and $|\langle a(\omega)\rangle|^2$ of H_2 calculated with the TDLB$_\alpha$ (black solid line and green $\times$) and TDSIC (red dashed line and blue circles) methods.

harmonics. The two methods agree reasonably well. The largest differences occur in the "multiphoton regime," in which the photon energy of the harmonic is less than the vertical ionization potential. The difference in the electronic structure obtained by the two TDDFT methods is the cause of the differences. The electronic structure difference is also reflected in the vertical I_p's shown in Fig. 1, calculated as the absolute value of energy of the highest occupied orbital. The TDLB$_\alpha$ functional is optimized to reproduce the full configuration-interaction (CI) I_p values; therefore we expect TDLB$_\alpha$ to be more accurate.

The minimum number of photons it takes to ionize is 11 at the equilibrium distance. The difference between the two methods is minimal above the 11th harmonic (H11) for $|a(R_{\rm eq},\omega)|^2$. The classical cutoff energy is given by $E_c = I_p + 3.17U_p$, with $U_p = F^2/4\omega_0^2$. In this case it is the 35th harmonic (H35). In our calculated spectrum in Fig. 2 H35 resembles a cutoff, as the peaks decrease to a minimum at H41. However, they increase again at H43 followed by a second plateau with a cutoff at H55. To explain the structure of H43 and above, we postulated the following two-electron dynamics mechanism [23]. While one electron tunnels out and gains a kinetic energy equivalent to $3.17U_p$, the ion experiences a multiphoton excitation from the $^2\Sigma_g^+$ ground state to the $^2\Sigma_u^+$ first excited state. Upon recombination, the H_2 molecule returns to the ground electronic state, releasing a photon that should be H43. Above H55 the second electron ionizes as well, blocking the two-electron mechanism of exciting one electron while ionizing the other. This is the reason for the second cutoff at H55. Note that this occurs only with the fixed-nuclei calculation at $R_{\rm eq}$.

The HHG results for $R_{\rm eq}$ and for the ground vibrational state differ substantially and particularly so at high harmonics. The second plateau of $|a(R_{\rm eq},\omega)|^2$ disappears. Overall $|\langle a(\omega)\rangle|^2$ is much lower, and the difference between $|a(R_{\rm eq},\omega)|^2$ and $|\langle a(\omega)\rangle|^2$ increases with ω. Close to H35, $|\langle a(\omega)\rangle|^2$ is smaller by two orders of magnitude than $|a(R_{\rm eq},\omega)|^2$. These comparisons suggest significant R dependence of $|a(R,\omega)|^2$.

To examine the R dependence of the dipole acceleration, we plot the magnitudes and phases of $a(R,\omega)$, calculated with the TDLB$_\alpha$ method, as a function of R in Fig. 3. Each curve corresponds to one harmonic emission. The TDSIC method produces similar features, although there are small quantitative differences as a result of different electronic structures [23].

Figure 3(a) shows the harmonics in the multiphoton regime. The amplitudes of the 5th–11th harmonics each have a peak near the multiphoton resonance between the ground and an excited state [23]. Accurate electronic structures of both the ground and excited states are needed in this regime. For the TDDFT method, the choice of a time-dependent exchange-correlation (TDXC) functional is crucial here. Between our two methods, the TDLB$_\alpha$ is more accurate.

The harmonics in Figs. 3(b) and 3(c) have energies higher than the vertical I_p. The slopes of the phases as functions of R are large here. Note that the phases are presented in units of 2π, which means that curves in Figs. 3(b) and 3(c) have 2–4 cycles of phase changes in the presented R range. Broad peaks are the main feature of $|a(R,\omega)|$ in Fig. 3(b). They are due to the multiphoton resonances that can be seen in Fig. 3(a).

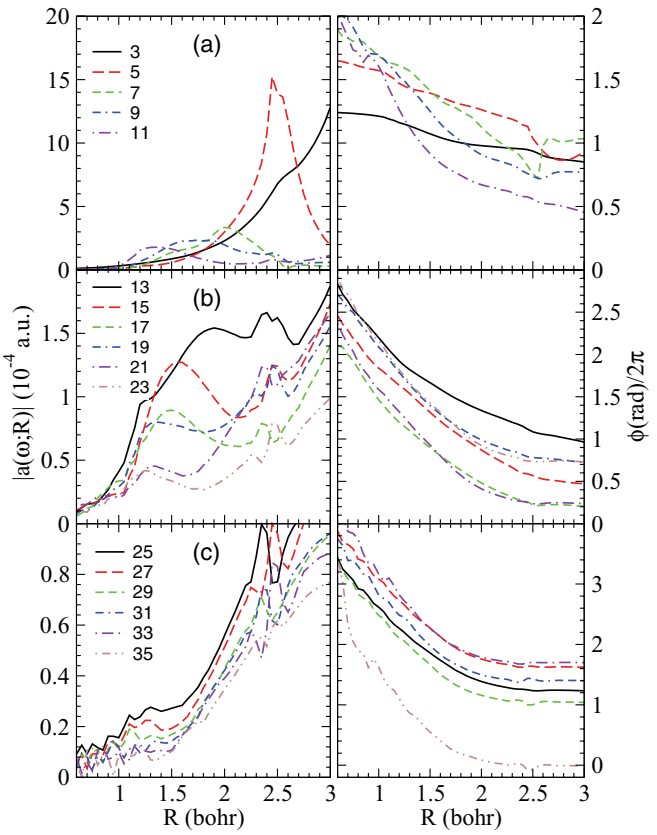

FIG. 3. (Color online) The amplitudes in atomic units and phases in units of 2π of $a(R,\omega)$ for $\omega = 3\omega_0,5\omega_0,\ldots,35\omega_0$, as a function of R, calculated with the TDLB$_\alpha$ method.

Values of $a(R,\omega)$ near $R = R_{\rm eq}$ make the largest contribution to $S(\omega)$.

Figure 3(c) shows the harmonics near the classical cutoff H35. The amplitude $|a(R,\omega)|$ increases by one order of magnitude between $0.5a_0$ and $3.0a_0$. This increase can be explained by the vertical I_p, which decreases for larger R. Multiphoton resonances and, possibly, two-photon processes cause structures in $|a(R,\omega)|$ at short distances and in the range from $2.2a_0$ to $2.5a_0$. For $R > 2a_0$, the slopes of the phases tend to zero, which is consistent with the decrease of the slope of I_p at larger R shown in Fig. 1. We also notice that the slopes of the phases in Fig. 3 increase with the harmonic order.

V. ISOTOPE-EFFECT CALCULATION

From the R-dependent dipole accelerations we compute $|\langle a(\omega)\rangle|^2$ and the spectral densities for the $v = 0$ vibrational states of D_2 and H_2 according to Eq. (14). The ratios of these spectral densities are shown in Fig. 4 (solid black line) up to the classical cutoff energy. Even though the vibrational wave function of D_2 is only slightly narrower than the H_2 wave function, as shown in Fig. 1, the rapid phase variation of $a(\omega,R)$ results in a larger spectral density for D_2. Except for H35, the ratio increases with the harmonic order. In Fig. 4 we also include the experimentally observed ratios and error bars that we took from Fig. 3(b) of the 2006 paper by Baker *et al.* [4]. These experimental results correspond to similar laser parameters: $\lambda = 775$ nm, an estimated intensity

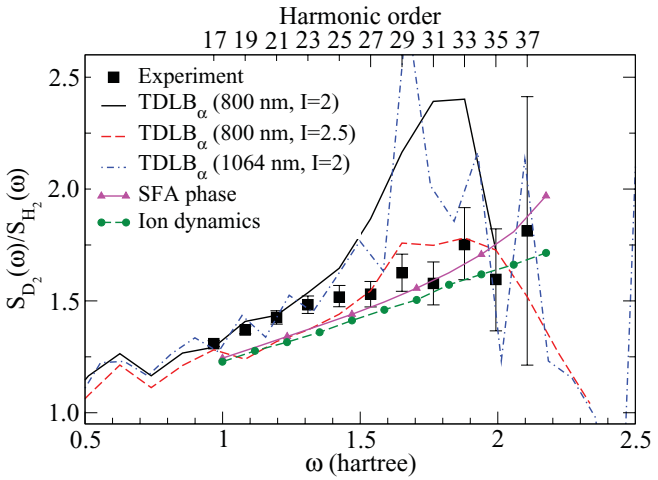

FIG. 4. (Color online) The D_2-to-H_2 spectral density ratios calculated with the TDLB$_\alpha$ method at two intensities, compared to experiment [4]. The black solid line and the dashed red line are calculated for 800 nm lasers. The blue dash-dotted line is for 1064 nm 2×10^{14} W/cm^2 lasers. The magenta line with triangles is the result of the SFA-phase model, and the green dashed line with circles is the result of Lein's ion-dynamics model [15]. The unit of intensity I is 10^{14} W/cm^2.

of 2×10^{14} W/cm^2, and a setup in which the harmonic signal is dominated by the so-called short trajectories [16]. For the lower harmonics the experimental error bars are the smallest and the agreement with our calculations is the best. Around H31 our calculated ratio is larger, but we also find that here the results are particularly sensitive to the parameters: increasing the laser intensity to 2.5×10^{14} W/cm^2 (the red dashed line) brings the calculated results close to the observed values. Also, changing the laser frequency to $\lambda = 1064$ nm (the blue dash-dotted line) mainly affects the results for the higher harmonics. Results for calculations with the TDSIC method are not shown, but we found that they are in close agreement with the TDLB$_\alpha$ results.

VI. A STRONG-FIELD-APPROXIMATION PHASE MODEL

Although the amplitude $|a(\omega,R)|$ also has a strong R dependence, it has a much smaller effect on the spectral density ratio (SDR) than does the phase. Ratios recalculated without the phase variation against R are very close to 1. We also notice that the phase variation shown in Fig. 3 agrees very well with a strong-field-approximation (SFA) expression [7,28]

$$\phi_{\rm SFA}(\omega,R) - \phi_{\rm SFA}(\omega,R_0) \approx [I_p(R) - I_p(R_0)]\tau(\omega). \quad (15)$$

Here $I_p(R)$ is the R-dependent vertical ionization potential (see Fig. 1) and $\tau(\omega)$ is the recollision time. This approximation has the advantage that it applies to the contribution from the short trajectories [16], matching the conditions of the available experimental data [4,5]. We thus make a relatively simple SFA model, in which we take the amplitude as R independent and obtain the R dependence of the phase using Eq. (15). The recollision time was included in Fig. 3(b) of Ref. [4]. With $\tau(\omega)$ from that figure, and the constant amplitude dropping out of the equation, we compute the SDR as

$$\frac{S_{D_2}(\omega)}{S_{H_2}(\omega)} = \left|\frac{\langle\chi_{D_2}(R)|e^{i\phi_{\rm SFA}(\omega,R)}|\chi_{D_2}(R)\rangle}{\langle\chi_{H_2}(R)|e^{i\phi_{\rm SFA}(\omega,R)}|\chi_{H_2}(R)\rangle}\right|^2. \quad (16)$$

The result is labeled the "SFA phase" in Fig. 4. It is in remarkably close agreement with experiment. We also include the original theoretical result which was obtained with the ion-dynamics theory of Lein [15]. In this theory the R dependence of phase and amplitude is not taken into account. Instead, the isotope effect arises from the nuclear motion of the H_2^+ ion while one electron is traveling in the continuum; we label the curve as "Ion dynamics."

Considering only the R-dependent phase and considering the ion dynamics but ignoring the R dependence seem to be two independent approaches, and yet the agreement between our SFA-phase model and Lein's ion-dynamics model suggest that they are intrinsically related. In the ion-dynamics model, the ion is assumed to move on the Born-Oppenheimer ground-state ion potential surface, which also determines the R-dependent phase in the SFA-phase model. Indeed Eq. (16) is equivalent to

$$\frac{S_{D_2}(\omega)}{S_{H_2}(\omega)} = \left|\frac{\langle\chi_{D_2}(R)|e^{-iI_p(R)\tau(\omega)}|\chi_{D_2}(R)\rangle}{\langle\chi_{H_2}(R)|e^{-iI_p(R)\tau(\omega)}|\chi_{H_2}(R)\rangle}\right|^2, \quad (17)$$

and $e^{-iI_p\tau}|\chi\rangle$ is a short-time approximation of the TD ion wave packet.

In a 2008 follow-up experiment by Baker *et al.* [5], the isotope effect on HHG in D_2 and H_2 was measured for a driving laser field of 800 nm with intensities of $(3.0\pm0.1)\times10^{14}$ and $(2.2\pm0.2)\times10^{14}$ W/cm^2 [5]. In Fig. 5 we show the experimental data from Figs. 1(a) and 1(b) of this paper as a function of the harmonic order. The results for the lower laser intensity [from Fig. 1(b)] are shown in black and for the higher intensities [from Fig. 1(a)] in red. Although the error bars sometimes overlap, the HHG isotope ratio seems to be higher for the lower intensity. Again, the SFA recollision times $\tau(\omega)$ were reported in the original work and we used

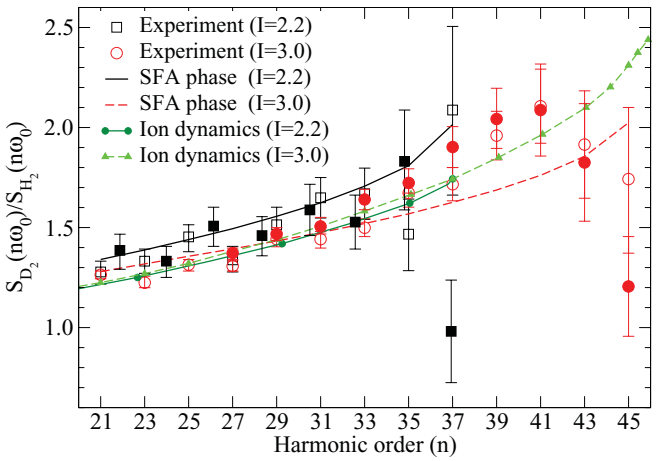

FIG. 5. (Color online) Comparison of the D_2-to-H_2 ratio calculated with the SFA-phase model with experimental data [5]. Note that there are two sets of experimental data for each intensity presented with the filled and unfilled symbols respectively. Results from the ion-dynamics calculations are also shown. The unit of intensity I is 10^{14} W/cm^2.

them in our SFA-phase model. The results are shown as a black solid line and a red dashed line for the lower and higher intensities. Up to H35 the results of the SFA-phase model are within the experimental error bars and reproduce the intensity dependence of the ratios very well. For higher harmonics the experimental error bars increase, but the ratios seem to drop above H41 for the experiment with the higher intensity. We note that our calculations with the TDLB$_\alpha$ method at 2.5×10^{14} W/cm^2 (Fig. 4) show a similar trend.

In Figs. 1(a) and 1(b) of Ref. [5] results for three different SFA-based theories were shown. The best results there are included in our Fig. 5; the solid dark green line with filled circles corresponds to the lower intensity and the dashed green line to the higher intensity. The intensity dependence of the experiment is not reproduced. This theory included the effect of the parent ion dynamics and a "dynamic two-center interference" effect. If either of these effects was not included no agreement with experiment was found. In Ref. [5] a scaling factor of 0.85 for the theoretical results was mentioned, which we do not include in our SFA-phase model. The SFA-phase model has better agreement with experimental data in this case, indicating that it is not simply an approximation of the ion-dynamics model. We look forward to seeing future experimental data on the intensity dependence of the isotope effect, which is predicted by the SFA-phase model but not the ion-dynamic model. So far this model allows us to make the following approximation for molecular HHG:

$$|a(\omega)|^2 \approx |\langle\chi|e^{iI_p(R)\tau(\omega)}|\chi\rangle|^2 |a(\omega,R_{\rm eq})|^2. \qquad (18)$$

Note that the factor $|\langle\chi|e^{iI_p(R)\tau(\omega)}|\chi\rangle|^2$ is equal to $|\langle\chi|e^{-iI_p(R)\tau(\omega)}|\chi\rangle|^2$. When $I_p(R)$ is flat and $\chi(R)$ is sharp, e.g., the case in which the molecule consists only of heavy atoms, this factor is close to 1. In our case, this formula agrees well with Eq. (14) up to H25 when $I = 2 \times 10^{14}$ W/cm^2. The difference is within 7%. For H27–H35, the difference elevates to 20%–40%. For larger intensity such as $I = 2.5 \times 10^{14}$ W/cm^2 the agreement is significantly improved. The amount of computation involved in this formula is significantly less than that of Eq. (14) and it reproduces the measured isotope effect as well as does the SFA-phase model. In addition, this formula applies not only to TDDFT but to other methods as well, including SFA methods.

From Eq. (18) it is clear that if the vertical I_p is not flat as a function of nuclear geometry around the equilibrium structure, then HHG should be a sensitive probe of the ground-state wave function. In our case it can distinguish the subtle difference between χ_{H_2} and χ_{D_2} vibrational wave functions shown in Fig. 1.

VII. PROBING NUCLEAR DYNAMICS

Since the HHG signal is particularly sensitive to the shape of the nuclear wave function of the molecule it can in principle be used as an ultrafast probe of nuclear dynamics. To illustrate this, we construct a time-dependent wave function $\chi(R,t) = c_0\chi_0(R) + e^{-i\Delta\epsilon t}c_1\chi_1(R)$, where χ_0 and χ_1 are the ground and first excited vibrational states of H_2, respectively, with energy difference $\Delta\epsilon$, and we substitute it in Eq. (14) to compute

$$|a(\omega,t)|^2 = |\langle\chi(R,t)|a(\omega,R)|\chi(R,t)\rangle|^2. \qquad (19)$$

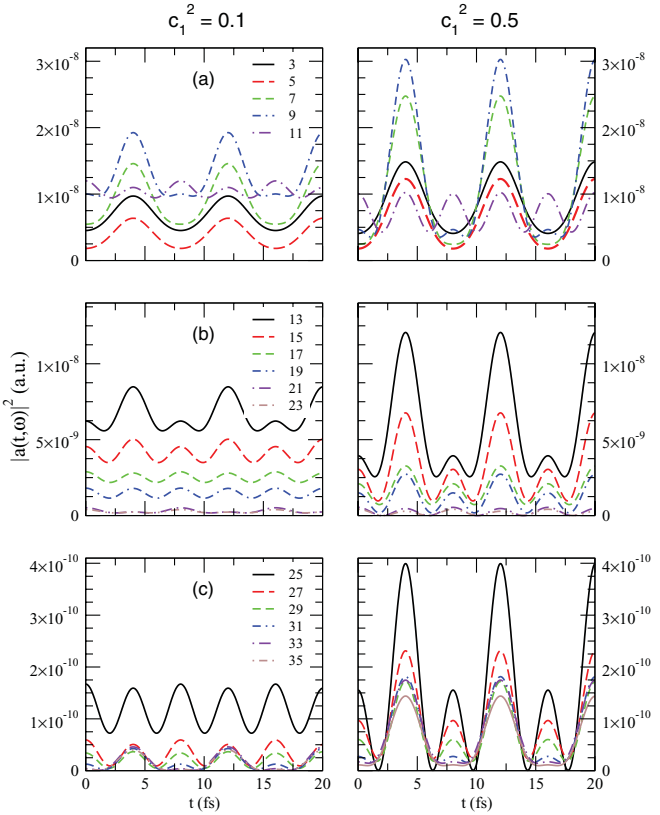

FIG. 6. (Color online) The dipole acceleration squared, $|a(t,\omega)|^2$, for harmonics $\omega = 3\omega_0, 5\omega_0, \ldots, 35\omega_0$, as a function of the delay time t between the preparation of the vibrational wave packet and the HH generating pulse. The three panels on the left correspond to a wave packet which consists of 10% $v = 1$ ($|c_1|^2 = 0.1$) and the panels on the right correspond to a wave packet with equal contributions for $v = 0$ and $v = 1$ vibrational states.

Note that the nuclear dynamics here is different from the ion dynamics in Lein's model, which we think is accounted for to a certain extent in Eq. (19). In Fig. 6 we plot $|a(\omega,t)|^2$ for $c_1^2 = 1 - c_0^2 = 0.1$ in the left panels and $c_1^2 = 0.5$ in the right panels. The vibrational period $T = 8$ fs. There are peaks at $t = T/2$ for H3–H35, and for H9 and above there are peaks at $t = T$ as well. The scale of oscillation increases with c_1^2 and roughly increases with the harmonic order as well. In particular, $S(33\omega_0,T/2)/S(33\omega_0,0.15T) = 48.9$ for $c_1^2 = 0.1$ and $S(25\omega_0,T/2)/S(25\omega_0,0.21T) = 577.9$ are the largest oscillations in the left and right panels, respectively.

VIII. SUMMARY

In summary we first benchmark a theory for HHG using experimental measurements of the isotope effect of the hydrogen molecule. In this theory the electronic and nuclear dynamics are separated and both are treated quantum mechanically. In such a treatment the dynamics of the ion during the HHG process, which depends on the harmonic order, is not described. Accurate description of the ion dynamics in intense fields requires full quantum treatment of both the nuclei and electrons, which is presently computationally unfeasible for molecules larger than H_2. Results of methods in which

electrons are treated by TDDFT reproduce experimental data up to H25, while H35 is the classical cutoff.

Our calculations indicate that the R-dependent phase is another factor that contributes to the isotope effect, as well as to the sensitivity to the nuclear wave function and dynamics. This phase factor can be modeled by using a SFA formalism. The SFA-phase model thus created reproduces experimentally measured data, including those for which the ion-dynamics model has to be further modified by a factor of dynamic two center interference. It resembles a short-time approximation of Lein's model, but originates from the R dependence of HHG rather than the ion dynamics. It differs from the ion-dynamics model in predicting the intensity dependence of the isotope effect. As such we recommend further experimental work to clarify this point. This model provides an empirical way for TDDFT methods to calculate the HHG of molecules. It involves much less computation than using Eq. (14). For hydrogen-containing molecules, it is likely to be more accurate in calculating harmonics that are near cutoff and a little less accurate for harmonics far below the cutoff.

ACKNOWLEDGMENTS

We acknowledge Dr. Johannes Feist for helpful discussions. This work is supported by the National Science Foundation Award No. PHY-0855676.

[1] A. McPherson, G. Gibson, H. Jara, U. Johann, T. S. Luk, I. A. McIntyre, K. Boyer, and C. K. Rhodes, J. Opt. Soc. Am. B **4**, 595 (1987).
[2] X. F. Li, A. L'Huillier, M. Ferray, L. A. Lompré, and G. Mainfray, Phys. Rev. A **39**, 5751 (1989).
[3] N. L. Wagner, A. Wuest, I. P. Christov, T. Popmintchev, X. Zhou, M. M. Murnane, and H. C. Kapteyn, Proc. Natl. Acad. Sci. USA **103**, 13279 (2006).
[4] S. Baker, J. S. Robinson, C. A. Haworth, H. Teng, R. A. Smith, C. C. Chirilă, M. Lein, J. W. G. Tisch, and J. P. Marangos, Science **312**, 424 (2006).
[5] S. Baker, J. S. Robinson, M. Lein, C. C. Chirilă, R. Torres, H. C. Bandulet, D. Comtois, J. C. Kieffer, D. M. Villeneuve, J. W. G. Tisch *et al*., Phys. Rev. Lett. **101**, 053901 (2008).
[6] W. Li, X. Zhou, R. Lock, S. Patchkovskii, A. Stolow, H. C. Kapteyn, and M. M. Murnane, Science **100**, 056404 (2008).
[7] H. Worner, J. Bertrand, D. Kartashov, P. Corkum, and D. Villeneuve, Nature (London) **466**, 604 (2010).
[8] M. Lewenstein, P. Balcou, M. Y. Ivanov, A. L'Huillier, and P. B. Corkum, Phys. Rev. A **49**, 2117 (1994).
[9] K. J. Schafer, B. Yang, L. F. DiMauro, and K. C. Kulander, Phys. Rev. Lett. **70**, 1599 (1993).
[10] P. B. Corkum, Phys. Rev. Lett. **71**, 1994 (1993).
[11] A. T. Le, X. M. Tong, and C. D. Lin, J. Mod. Opt. **54**, 967 (2007).
[12] B. K. McFarland, J. P. Farrell, P. H. Bucksbaum, and M. Ghr, Science **322**, 1232 (2008).
[13] O. Smirnova, Y. Mairesse, S. Patchkovskii, N. Dudovich, D. Villeneuve, P. Corkum, and M. Y. Ivanov, Nature (London) **460**, 972 (2009).
[14] M. A. L. Marques, N. T. Maitra, F. M. da Silva Nogueira, E. K. U. Gross, and A. Rubio, *Fundamentals of Time-Dependent Density Functional Theory*, Lecture Notes in Physics, Vol. 837 (Springer, Heidelberg, 2012).
[15] M. Lein, Phys. Rev. Lett. **94**, 053004 (2005).
[16] P. Antoine, A. L'Huillier, and M. Lewenstein, Phys. Rev. Lett. **77**, 1234 (1996).
[17] X. Chu and Shih-I Chu, Phys. Rev. A **63**, 023411 (2001).
[18] X. Chu and Shih-I Chu, Phys. Rev. A **64**, 063404 (2001).
[19] X. Chu and Shih-I Chu, Phys. Rev. A **70**, 061402(R) (2004).
[20] D. A. Telnov and Shih-I Chu, Phys. Rev. A **80**, 043412 (2009).
[21] X. Chu, Phys. Rev. A **82**, 023407 (2010).
[22] X. Chu and M. McIntyre, Phys. Rev. A **83**, 013409 (2011).
[23] X. Chu and P. J. Memoli, Chem. Phys. **391**, 83 (2011).
[24] P. R. T. Schipper, O. V. Gritsenko, S. J. A. van Gisbergen, and E. J. Baerends, J. Chem. Phys. **112**, 1344 (1999).
[25] D. T. Colbert and W. H. Miller, J. Chem. Phys. **96**, 1982 (1992).
[26] G. C. Groenenboom and D. T. Colbert, J. Chem. Phys. **99**, 9681 (1993).
[27] W. Kołos and L. Wolniewicz, J. Chem. Phys. **43**, 2429 (1965).
[28] T. Kanai, E. J. Takahashi, Y. Nabekawa, and K. Midorikawa, Phys. Rev. Lett. **98**, 153904 (2007).